Water adsorption in fresh and thermally aged zeolites: equilibrium and kinetics

Beatriz O. Nascimento[1] · Bianca F. dos Santos[1] · Débora A. S. Maia[1] · Darley C. de Melo[2] · Enrique Vilarrasa-Garcia[1] · Antônio Eurico B. Torres[1] · Moisés Bastos-Neto[1] · Diana C. S. Azevedo[1]

Abstract

Zeolites are widely employed in the industrial drying of gases by Temperature Swing Adsorption (TSA). In a typical TSA process, the adsorbent is packed in a fixed bed, which is sequentially subjected to a "cold" feed (adsorption) and a hot flush (desorption). Due to the hydrothermal stress, adsorbents may suffer from reduced drying capacity in long-term service. The aim of this work is to assess the impact of thermal aging of two zeolite materials (LTA and CHA) having similar pore openings but different Si/Al ratios. We examined how simulated thermal aging affected porous texture, coke deposition and water vapor adsorption equilibrium and kinetics. Both zeolites showed reduced uptake of probe molecules (N_2 at 77 K and CO_2 at 273 K) and water vapor (303 K) when subjected to simulated thermal aging. In Fourier-Transform Infrared Spectroscopy (FTIR) analyses, only the aged LTA zeolite showed bands related to the presence of aromatic compounds. Water vapor adsorption uptake decreased 28.6% and 18.4% for LTA and CHA at 30 mbar, respectively. Kinetic studies indicate a reduction in water diffusion coefficient after the aging cycles. Although LTA has a significantly higher affinity for water as compared to CHA, the latter is much more resistant to hydrothermal aging with comparatively faster water diffusion.

Keywords Water adsorption · Kinetic model · Deactivation · Characterization · Zeolite

Symbols

a	Conglomerate external surface area per unit volume (m^{-1})
C_{ps}	Solid specific heat capacity ($J\,kg^{-1}\,K^{-1}$)
C_{pw}	Water specific heat capacity ($J\,kg^{-1}\,K^{-1}$)
$\overline{C_p}$	Specific heat capacity average ($J\,kg^{-1}\,K^{-1}$)
D_μ	Diffusion coefficient ($m^2\,s^{-1}$)
D_μ^0	Corrected diffusion coefficient ($m^2\,s^{-1}$)
$D_{\mu,b}^0$	Diffusion coefficient in a reference temperature ($m^2\,s^{-1}$)
ΔH_{ads}	Adsorption enthalpy ($J\,mol^{-1}$)
Δt	Time interval to achieve the final pressure (s)
E_a	Adsorption activation energy ($J\,mol^{-1}\,K^{-1}$)
h_f	Heat transfer coefficient ($W\,m^{-2}\,K^{-1}$)
P	Pressure (Pa)
P_b	Phase bulk pressure (Pa)
P_{bi}	Phase bulk initial pressure (Pa)
P_f	Final pressure (Pa)
P_i	Initial pressure (Pa)
q	Adsorbed amount ($mol\,kg^{-1}$)
q_s	Maximum adsorbed amount ($mol\,kg^{-1}$)
$\overline{q}$	Volumetric average adsorbed amount ($mol\,kg^{-1}$)
r	Radial coordinate (m)
R	Particle radius (m)
R_{IG}	Universal gas constant ($J\,mol^{-1}\,K^{-1}$)
ρ_s	Solid specific volume ($kg\,m^{-3}$)
t	Time (s)
T	Temperature (K)
T_b	Phase bulk temperature (K)

✉ Diana C. S. Azevedo
diana@gpsa.ufc.br

1 GPSA, Chemical Engineering Department, Universidade Federal do Ceará, Campus do Pici, bl. 731, Fortaleza, Ceará 60760-400, Brazil

2 PETROBRAS/CENPES, Rio de Janeiro, RJ 21941-915, Brazil

1 Introduction

Water vapor is one of the contaminants present in raw natural gas which have to be removed prior to other unit operations. Even though it is present in small quantities, it can generate issues during transportation and processing, the most severe being the build-up of gas hydrates that may

block pipelines and equipment. Moreover, water reduces the heating value of natural gas and may condense in pipelines, resulting in erosion and corrosion, especially in the presence of acid contaminants, such as carbon dioxide and hydrogen sulfide [1, 2].

Therefore, gas drying is an essential step during natural gas processing, which is usually carried out by adsorption on molecular sieves when very low water contents are required (typically 0.1 ppm or less) [3]. Among the variety of drying adsorbents available, molecular sieves stand out due to their well-defined pore structure that allows for the selective adsorption of the molecule of interest [1]. The strong affinity for water, which results mainly from the local electrostatic fields, makes the zeolitic molecular sieves the most used adsorbent industrially for dehydration [4].

Linde Type A (LTA) zeolites are the most frequent options for drying in the natural gas industry. In this class of materials there are zeolites 3A (exchange cation: potassium), 4A (exchange cation: sodium) and 5A (exchange cation: calcium) [5]. Chabazite (CHA) is another interesting option, with pore windows similar in diameter to those of LTA. However, LTA has larger cages (alpha super cage) and a fraction of its cations are not directly accessible to the host molecules, whereas CHA cations are totally accessible [6].

Natural gas drying by adsorption is usually carried out by TSA process, which alternates "cold" and "hot" steps in cycle to adsorb and desorb water, respectively. During cycling, the molecular sieve is exposed not only to temperature swings, but also to humidity and the presence of lower contents of heavy hydrocarbons. This combination may lead to a slow and irreversible breakdown of the crystal structure, resulting in adsorbent deactivation [7]. Such deactivation may also occur as a result of coke formation, that commonly appears when reactive hydrocarbons are submitted to high temperatures during a regeneration step [8]. A preliminary study carried out by our group [9], proposed a simulated aging protocol to emulate TSA conditions. Understanding adsorbent deactivation as a consequence of operating conditions entails the study of both equilibrium and kinetics data. Adsorption capacity is investigated by equilibrium isotherms, whereas the resistances imposed to the transport of adsorbate and heat into adsorbent particles is investigated by kinetic models [7, 10]. A simple and interesting option to study kinetics is the description of uptake curves in gravimetric devices by applying mass and heat balance equations [11].

Thus, the aim of this work is to elucidate how water adsorption is affected in the scenario of natural gas drying by emulating TSA process conditions (aging protocol) and comparing the performance of two zeolite molecular sieves (LTA and CHA) with the support of a variety of characterization techniques. Another goal of the present work is to estimate kinetic data (water diffusivity) as an important input parameter for TSA process design. For this purpose, a mathematical model based on mass and energy balances was proposed and solved in Gproms ModelBuilder (Process Systems Enterprise Inc., UK).

2 Experimental

2.1 Materials

Two zeolite molecular sieves were used in this work for the aging tests. They are a synthetic zeolite type 4A (LTA, Sigma Aldrich) with sodium as exchange cation and a natural zeolite type chabazite (CHA), available as cylindrical pellets, previously reported in Santiago et al. [9]. Both adsorbents were shaped as pellets with 1.6 mm diameter.

2.2 Aging test

The aging tests were performed following the methodology reported by Santiago et al. [9]. The assays were conducted in a 500-mL stainless-steel vessel (Parr Instrument Company, USA) loaded with 25 g adsorbent. First, the zeolite was humidified at 303 K for 24 h by continuously flowing a water-saturated N_2 stream coming from a washing vessel at 308 K. Then, liquid n-heptane was added at a volume/mass ratio of 0.6 mL g^{-1} to account for long chain hydrocarbons ordinarily present in natural gas. Then, the Parr reactor was pressurized up to 30 bar with a mixture of CO_2 and CH_4 (1:4 vol.) for an hour. Afterwards, the reactor was heated up to 523 K, at a rate of 3 K min^{-1}, and was kept at this temperature for 3 h. Then, the reactor was cooled down to 303 K by natural convection. These heating/cooling steps went on and samples were collected after 35 cycles. The aged samples were assigned by A35, following the term LTA or CHA.

2.3 X-ray diffraction

The X-Ray diffraction patterns for the zeolite samples were conducted in an X'PERT PRO Powder diffractometer (PANalytical, UK) which was equipped with a Co-Kα anode. The wavelength, λ, equal to 1.7889 Å and the 2θ range was 5° and 70°.

2.4 X-ray fluorescence

Chemical analysis using the technique of X-Ray Fluorescence (XRF) was carried in an ARL ADVAN'XP (Thermo, EUA). The bulk composition of the zeolite samples was expressed by elements and conducted in Helium atmosphere.

2.5 Textural characterization

N_2 adsorption/desorption isotherms at 77 K and CO_2 adsorption isotherms at 273 K were measured in an Autosorb-iQ3 instrument (Quantachrome, EUA). Both adsorbate gases were supplied by White Martins Praxair Inc. with purities of 99.999 and 99.8% for N_2 and CO_2, respectively. The typical samples size weighed about 100 mg before degassing at 573 K under vacuum (10^{-5} bar) for 10 h. Equilibrium was assumed for pressure variations smaller than 0.001 torr in 10 min as recommended by the instrument manufacturer. Nitrogen adsorption/desorption isotherms were used to calculate the apparent BET specific surface area, within the relative pressure range between 0.05 and 0.3. The micropore volume was obtained by the application of the Dubinin–Radushkevich (DR) equation to both N_2 and CO_2 adsorption isotherm data [4].

2.6 Fourier-transform infrared spectroscopy

The Fourier-Transform Infrared Spectroscopy (FTIR) analysis of the samples was obtained using a spectrometer VERTES 70 (Bruker, UK). The materials were conformed in tablets with KBr.

2.7 Elemental analysis CHN

The amounts of carbon, hydrogen and nitrogen were determined by elemental analysis in a CHNS 932 analyzer (LECO, Germany).

2.8 Thermogravimetric analysis

The thermogravimetric analysis (TGA) measured the mass losses and volatile compounds release from sample upon heating in inert atmosphere. These analyses were performed in an STA 409 CD/403/5/G SKIMMER (Netzsch, Germany). The samples were heated at a rate of 10 K min^{-1} until 1072 K, under a constant nitrogen flow rate of 20 mL min^{-1}.

2.9 Water vapor adsorption isotherm at 303 K

The water vapor isotherms were measured using an Intelligent Gravimetric Analyzer—IGA (Hiden Isochema Ltd., UK). The system is fully automated, comprising a microbalance, pressure and temperature regulators and an ultra-high vacuum (UHV) system. The microbalance has a stability of ± 1 μg and a weighting resolution of 0.2 μg. In the experiments, typically 23 ± 1 mg samples were loaded to the measuring chamber. Prior to isotherm measurements, the sample was degassed at 573 K under vacuum (10^{-6} mbar) for 8 h. Water vapor was generated using liquid deionized water placed in a vial, which was degassed by repeated evacuation

to generate the desired water vapor pressures. In the adsorption/desorption experiments, pressure ranged between 0.25 and 40 mbar at 303 K. The saturation pressure at this temperature, determined by the Antoine equation, is 42.5 mbar.

The IGA system software (by Hiden, UK) is provided with a kinetic analysis model which estimates, by monitoring the uptake curve in real time, the trend in the mass equilibrium values. This model has parameters like relaxation (percentage of variation between the measured and estimated values) and error tolerance that can be tuned for each sample. The equilibration time ranges between 20 min to 14 h, depending on the sample nature and the water partial pressure step assigned as set point. the measuring cell is thermostated by a water-cooling bath to ensure isothermal operation with ± 0.5 K variation. The sample temperature was controlled by computer software and the primary sensor is a thermocouple placed 5 mm away of the sample holder. The recorded mass gain as a function of time for a given step in water vapor pressure (0–0.25 mbar) was used to estimate the diffusion coefficient of each sample by fitting data to a mathematical model as explained in the following section.

2.10 Mathematical model

Considering that the mass diffusion in this system is described by Fick's Law and is limited by mass transfer inside the pellet [10], a differential mass balance for a cylindrical particle can be written as (only radial flow):

$$\frac{\partial q}{\partial t} = \frac{1}{r}\frac{\partial}{\partial r}\left(rD_\mu\frac{\partial q}{\partial r}\right) \tag{1}$$

where q is the concentration of the adsorbed phase, r is the radial position and D_μ is the diffusion coefficient, which may depend on the adsorbed concentration and the temperature.

The diffusivity, D, shown in Eq. (1), must be corrected by the thermodynamic factor (Eq. 2). This correction is a derivate of the equilibrium isotherms and it is related to the non-linearity between the activity and concentration [12]. The Langmuir Model was chosen to describe adsorption equilibrium and provided the thermodynamic factor, as presented in Eq. (2). In the Henry's Law domain, at sufficiently low loadings, the diffusivity remains constant, but as the adsorbed concentration increases, the diffusion coefficient may increase significantly.

$$D_\mu = D_\mu^0 \frac{\partial \ln P}{\partial \ln q} = \frac{D_\mu^0}{1 - q/q_s} \tag{2}$$

where D_μ^0 is the corrected diffusivity and q_s is the maximum adsorbed concentration in the Langmuir model (mmol g^{-1}).

Temperature dependency of the corrected diffusivity is assumed to follow Arrhenius' Law:

$$D_\mu^0 = D_{\mu,b}^0 \exp\left[\frac{E_a}{R_{IG}T_b}\left(1 - \frac{T_b}{T}\right)\right] \tag{3}$$

where $D_{\mu,b}^0$ (m^2 s^{-1}) is the diffusivity in a reference temperature and E_μ is the activation energy (J mol^{-1} K^{-1}).

Applying the initial and the boundary conditions and solving Eq. (1) gives us the loading at each radial position and time. The volumetric average concentration is given by:

$$\overline{q} = \frac{2}{R^2}\int_0^R rq(r,t)dr \tag{4}$$

where R is the particle radius.

Because of its exothermic character, adsorption releases energy to the surroundings, which might cause a rise in temperature within the particle and slightly shift local equilibrium. Therefore, it is necessary to add an energy balance to the model [10]. The term on the left-hand side of Eq. (5) corresponds to the energy accumulation in the adsorbent pellet/particle; on the right-hand side, the first term accounts for the energy generated due to adsorption and the second term is the heat dissipated to the surroundings.

$$\rho_s\overline{C_p}\frac{dT}{dt} = (-\Delta H_{ads})\rho_s\frac{d\overline{q}}{dt} - h_f a(T - T_b) \tag{5}$$

where ρ_s is the solid density (kg m^3), C_p is the mean heat capacity of material (J kg^{-1} K^{-1}), $-\Delta H_{ads}$ is the adsorption enthalpy for the system water on zeolite (J mol^{-1}), h_f is the heat transfer coefficient (W m^{-2} K^{-1}), a is the heat transfer surface of particles conglomerate and T_∞ is the temperature of the bulk gas phase (K).

The pressure is kept in the set point value by a system of valves and it is monitored by the transducers. The rise in pressure from the initial value to the set point is described by:

$$P(t) = \frac{P_f - P_i}{\Delta t} \tag{6}$$

where P_f is the set point pressure, P_i is the initial pressure and Δt is the time interval to achieve the pressure set point.

Initial and Boundary Condition The mass balance requires two boundary conditions: (Eq. 7) the symmetry condition, at r = 0, where the mass flux is null; and (Eq. 8) the equilibrium condition at the outer surface, as given by the Langmuir model.

$$r = 0; \quad \frac{\partial q}{\partial r} = 0 \tag{7}$$

$$r = R; \quad q = q_b = f(P_b) \tag{8}$$

Assuming the loading is the equilibrium condition with the initial pressure in time equal to zero:

$$t = 0; \quad q = q_i = f(P_{bi}) \tag{9}$$

The energy balance needs only one initial condition, which is the system initial temperature, 303 K. The model parameters are summarized in Table 1.

By solving the system of equations with the initial and boundary conditions and comparing it with experimental data, it is possible to extract kinetic information, such as the diffusivity ($D_{\mu,b}^0$). The mathematical model was solved in the gPROMS platform (Process System Enterprise, UK) and the method of discretization was based on centered finite differences (CFDM). In this work, bed effects were neglected due to the small sample size and the adsorbent pellet shape, which prevents particle agglomeration [13].

3 Results and discussion

3.1 X-ray diffraction

In Fig. 1, the X-Ray diffraction patterns of the two fresh (non-aged) zeolite samples are shown and compared to the data obtained in International Zeolite Association (IZA) [14] for structures LTA and CHA. The LTA sample is in very good agreement with the literature data. In the CHA sample, most reflections match those of the IZA reference, although

Table 1 Model parameters in Eqs. (1) to (9)

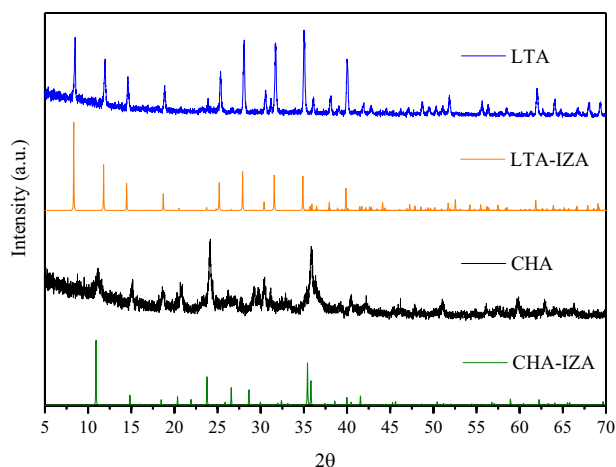| Parameter	Value	References
Particle radius R (m)	0.016	
Mean heat capacity $\overline{C_p}$ (J kg^{-1} mol^{-1})	$\overline{C_p} = C_{ps} + \overline{q_\mu} \cdot C_{pw}$	Dawoud et al. [40]
LTA Heat capacity C_{ps} (J kg^{-1} mol^{-1})	938.0	Qiu et al. [41]
CHA Heat capacity C_{ps} (J kg^{-1} mol^{-1})	1070.4	Chipera et al. [42]
Adsorption enthalpy of water in LTA ΔH_{ads} (J mol^{-1})	90,000	Wang [35]
Adsorption enthalpy of water in CHA ΔH_{ads} (J mol^{-1})	81,300	Jänchen et al. [43]
Density of the zeolite (LTA/CHA), ρ_s (kg m^{-3})	704	Dawoud et al. [40]
Activation Energy of LTA E_a (J mol^{-1})	32,410.0	Dawoud et al. [40]
Activation Energy of CHA E_a (J mol^{-1})	28,032.8	Barrer and Fender [44]

Fig. 1 Diffraction pattern of the LTA and CHA samples

Fig. 2 Nitrogen adsorption isotherm at 77 K for the LTA and CHA samples fresh and aged after 35 cycles. Data for CHA and CHA-A35 previously published in Santiago et al. [9]

Table 2 Elementary composition obtained by XRF analysis

Element	Sample (wt%)	
	LTA	CHA
Si	17.17	26.7
Al	12.34	8.4
Na	10.66	1.3
Mg	1.86	0.65
P	0.207	–
S	0.050	0.049
Cl	–	0.94
K	0.86	0.85
Ca	0.61	2.45
Ti	0.074	0.15
Mn	0.0078	–
Fe	0.86	5.4
Cu	0.016	–
Zn	0.011	–
Sr	–	0.47
Zr	0.017	0.098
Pb	0.032	–
Sn	0.11	0.911
Cs	–	0.147
Ba	0.14	1.55

Table 3 Textural properties of the LTA and CHA samples

Sample	BET area ($m^2 g^{-1}$)	Pore volume ($cm^3 g^{-1}$)	DR volume (N_2) ($cm^3 g^{-1}$)	DR volume (CO_2) ($cm^3 g^{-1}$)
LTA	39	0.094	0.010	0.180
LTA-A35	25	0.087	0.006	0.084
CHA	398*	0.280*	0.160*	0.148
CHA-A35	300*	0.230*	0.110*	0.104

*Previously reported in Santiago et al. [9]

CHA samples were equal to 1.34 and 3.05, respectively. The XRF technique takes into account the presence of other solid phases, such as the pellet binder and contaminants, so that the Si/Al ratios reported in Table 2 may be slightly different from those of the pure zeolite crystals. The major cation present in the LTA sample is sodium whereas it is calcium for the CHA sample. Note that a variety of other metals were identified in both samples as contaminants (maybe introduced by the binder). Fe and Ba outstand for sample CHA, which is in agreement with the XRD pattern of this sample and corroborates its natural occurrence.

3.3 Textural characterization

Nitrogen adsorption isotherms at 77 K are shown in Fig. 2 for the LTA and CHA samples. The CHA samples showed type II isotherms, which are characteristic of microporous materials with the presence of macropores [16]. Its BET surface area (shown in Table 3) is comparable to other natural CHA samples reported in the literature [17]. On the other hand, LTA samples showed a much lower N_2 adsorption capacity when compared to the CHA samples. It is well

there are other reflections, very likely associated to the presence of substances other than the aluminosilicate framework.

3.2 X-ray fluorescence

The X-Ray fluorescence data for the LTA and CHA samples are presented in Table 2. This analysis shows the bulk composition of zeolites and provide some information, as the bulk ratio Si/Al, presence of contaminants, cations identification, among others [15]. The Si/Al ratio to the LTA and
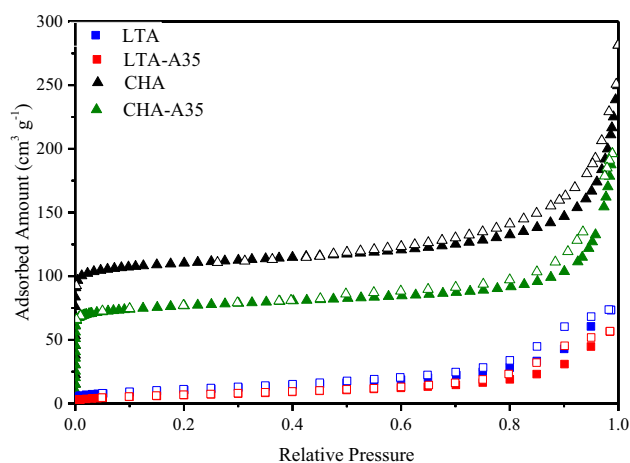
documented that Na-LTA (also known as zeolite 4A) displays kinetic restrictions to the diffusion of nitrogen molecules at cryogenic temperatures [18–21]. Therefore, the low adsorption uptakes found for LTA samples (Fig. 2) could be attributed to the adsorption on binder macropores. Carbon dioxide isotherms at 273 K are an alternative due the much higher temperature, which enhances the micropore diffusion despite the quadrupole effect of this probe molecule [16, 20].

Figure 3 shows the carbon dioxide adsorption isotherms at 273 K for fresh and aged LTA and CHA samples. The micropore volume was calculated based on these isotherms using the DR equation. Fresh CHA samples show good agreement between the volume calculated based on the nitrogen isotherm and on the CO_2 isotherms, which might indicate easy N_2 diffusion within the zeolite crystals. After the aging test, there is a decrease in adsorption capacity in both samples, which suggests partial deterioration in textural properties on both materials. For both samples, the decay in uptake upon aging is much more pronounced for CO_2 isotherms than N_2 isotherms.

Textural properties of fresh and aged samples are summarized in Table 3. The LTA-A35 sample shows a reduction of 36% in BET area and about 7% in total pore volume. These results were probably related to the blocking effect of n-heptane (as such or polymerized) in the macropores of the pellet adsorbent, because N_2 does not access most of the micropores. The reduction in the micropore volume, as sensed by CO_2 adsorption isotherms, was much higher (53%), which suggests that the micropore domain was significantly affected by the thermal aging protocol. The nitrogen adsorption isotherms and calculated BET surface area, total pore and micropore volumes for the CHA samples have been reported in Santiago et al. [9]. These results showed decreases of about 25, 18 and 30% for BET area, total pore volume and micropore volume, respectively. The reduction
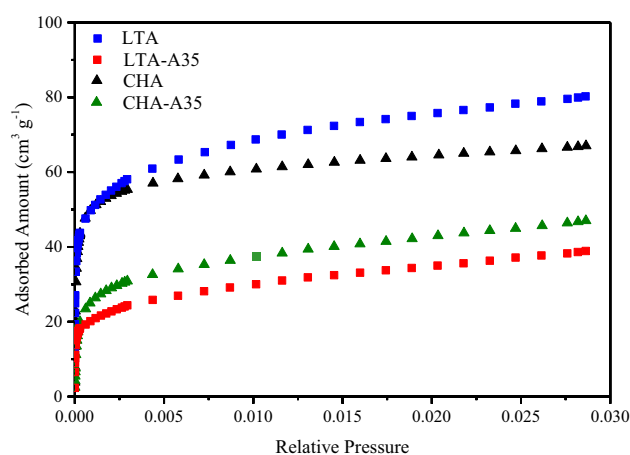
in the micropore volume from N_2 isotherms has the same order of magnitude as that calculated from CO_2 isotherms. These results point towards a higher resistance of CHA zeolite to hydrothermal aging, as compared to LTA zeolite, which may be due to the higher Si/Al ratio of the former.

3.4 Fourier-transform infrared spectroscopy

FTIR spectra of the fresh samples are depicted in Fig. 4. The LTA sample shows bands around 3943 and 1655 cm^{-1}, which was associated with water vibrations modes [22]. The tetrahedra TO$_4$ (where T is either a silicon or an aluminum atom) is the building block of all zeolites, which is assigned to the bands at 1002 and 674 cm^{-1} corresponding to asymmetric and symmetric stretch, respectively, whereas the band at 468 cm^{-1} is associated with the group deformation [22, 23]. LTA structure was signaled by the bands at 562 and 380 cm^{-1}, which are related to the vibration modes of the group DR4 (double 4-membered ring) characteristic of the LTA cubic structure [24].

In the FTIR spectrum of CHA, the bands at 3605 and 3440 cm^{-1} were associated to water, due to stretching vibrations of hydrogen atoms and hydroxyl groups, respectively. The band at 1645 cm^{-1} was related to the deformation of water molecules. Similar to LTA, the asymmetric stretching of TO$_4$ units appears at 1044 cm^{-1} and the symmetric stretching at 776 cm^{-1}. TO$_4$ deformations also have bands at 462 and 419 cm^{-1}. The bands at 638 and 521 cm^{-1} were assigned to the internal and external vibrations of the DR6 (double 6-membered rings) [25, 26].

After the aging protocol, the FTIR spectra of the samples showed new functional groups that are compatible with coke formation within pores or on macropore and external surface. In Fig. 5, FTIR spectra are zoomed in the range of 1300
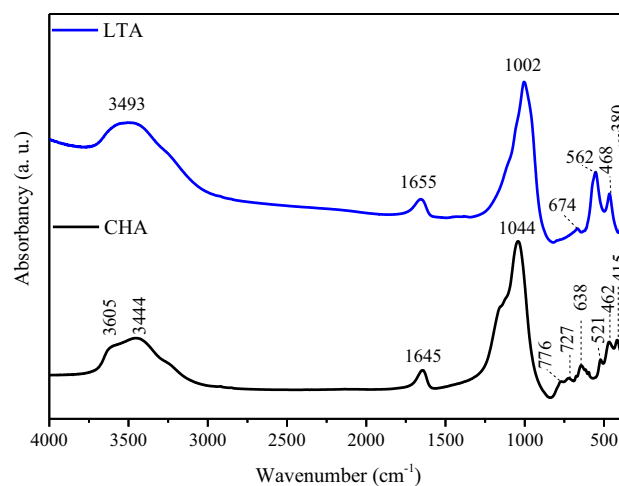

Fig. 3 Carbon dioxide adsorption isotherms at 273 K for the LTA and CHA fresh and aged samples

Fig. 4 FTIR spectrum for fresh samples of LTA (top) and CHA (bottom)

to 3000 cm^{-1} for the fresh and aged LTA samples. The range between 2800 and 3000 cm^{-1} usually shows bands related to aliphatic organic compounds, whereas aromatic and unsaturated compounds have characteristic bands in the range of 1300 and 1700 cm^{-1} [27]. For the aged LTA spectrum, the presence of linear hydrocarbons is suggested by the presence of bands at 2966 and 2936 cm^{-1}, related to the asymmetric stretching of CH$_2$ and CH$_3$ groups, respectively [28]. The band at 1569 cm^{-1} was ascribed to the stretching of double bonds in the aromatic ring and the band in 1466 cm^{-1} was associated to the presence of alkyl substitutions on the aromatic ring [29]. The bands at 1423 cm^{-1} refer to carbonate asymmetric stretch and to the presence of carbonate-like species at 1380 cm^{-1} [30]. All these bands were related to the aging process and suggest the fixation of organic aliphatic and aromatic molecules to the zeolite structure.

In Fig. 6, the same zoomed spectral region is shown of fresh and aged CHA samples. The aged sample presents asymmetric stretch to CH$_2$ groups at 2962 cm^{-1} and CH$_3$ groups at 2929 cm^{-1}. The symmetric stretch bands appear at 2877 cm^{-1} for the CH$_2$ groups and 2850 cm^{-1} for the CH$_3$ groups. Deformation vibration bands attributed to alkyl groups could be identified at 1464 and 1383 cm^{-1} corresponding, respectively, to ethyl and methyl groups [28]. The absence of the bands associated with the aromatic compounds might indicate that the chabazite structure is less prone to developing this type of coke, possibly due to less surface acidity caused by a higher Si/Al ratio. Additionally, LTA has larger internal cages (alpha super cage) than CHA zeolite, which may promote condensation reactions to form alkyl-aromatics and PAHs (polycyclic aromatic compounds). These species may accumulate and block the pores, thus deactivating the zeolite [29].
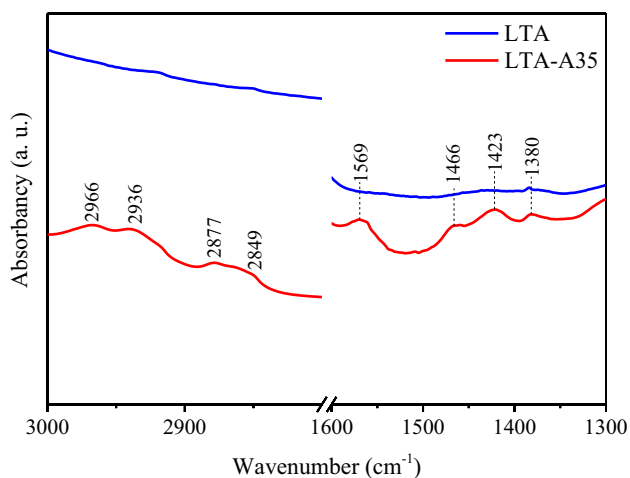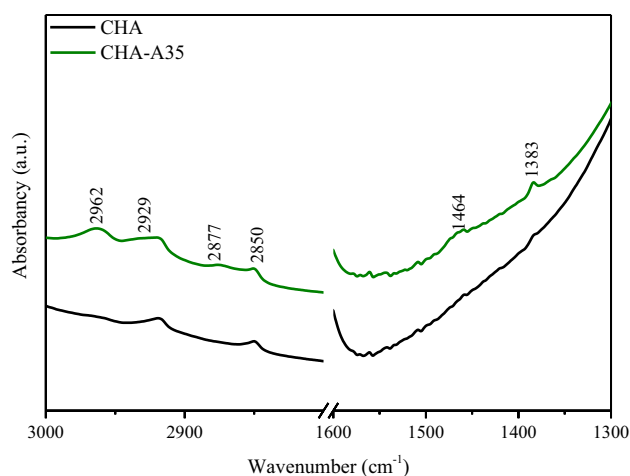

Fig. 6 FTIR analysis to the CHA fresh and aged samples after 35 cycles in the range of 1300 to 1600 cm^{-1} and 2800 to 3000 cm^{-1}

3.5 Elemental analysis

Table 4 condenses the data obtained from CHN elemental analysis, to check the bulk concentration of carbon as a consequence of the aging protocol. Xiong et al. have already used elemental analysis to study the formation and evolution of coke during the thermal treatment of bio-oil [31]. The total C concentration of the fresh samples was found to be very low (around 0.2%) and possibly due to sample manipulation. The increase of carbon content in aged samples is evident, and it was not observed when the aging protocol was carried out in absence of n-heptane [9]. This indicates that n-heptane probably accumulates in the pores of the material or reacts to form (alkyl)aromatic compounds under the influence of confinement effects and local acidity, which results in coke deposition, as evidenced by the FTIR results. Note that the amount of carbon is very similar in both aged LTA and CHA, but FTIR results suggest that aromatic compounds are not present in CHA-A35 and the C (%) content may be merely due to adsorbed n-heptane.

Fig. 5 FTIR analysis to the LTA fresh and aged sample after 35 cycles in the range of 1300 to 1600 cm^{-1} and 2800 to 3000 cm^{-1}

Table 4 Elemental analysis for the fresh and aged samples of LTA and CHA

Sample	C (%)	H (%)	N (%)
LTA	0.202	1.898	0.075
LTA-A35	2.202	1.994	0.008
CHA	0.195*	1.253*	0.019*
CHA-A35	2.354*	1.356*	0.095*

*Previously reported in Santiago et al. [9]

3.6 Thermogravimetric analysis

In Fig. 7, TGA and DTG curves are shown for the fresh and aged zeolite samples. For the fresh LTA zeolite, there is a mass loss event at 473 K, preceded by a shoulder (in DTG curve), which are related to water desorption. Then, the slower mass loss from 500 to 700 K is probably due to structural water bonds that are broken and the rupture of the hydroxyl groups [32]. The fresh CHA sample showed a similar but much smoother pattern of mass losses, with visible events only from the DTG curve. The aged samples show different patterns of mass loss when compared to the fresh samples. In the DTG curves of the aged samples, as compared to their fresh counterparts, there are more significant losses beyond 500 K, though the peaks are broad and ill-defined, which might be associated with the presence of new thermally resistant compounds in the cages and adsorbent pores. For the aged LTA sample, the reduction in intensity of the shoulder and peak below 500 K suggests that the water adsorption is reduced with respect to the fresh samples, which is not as evident for CHA.
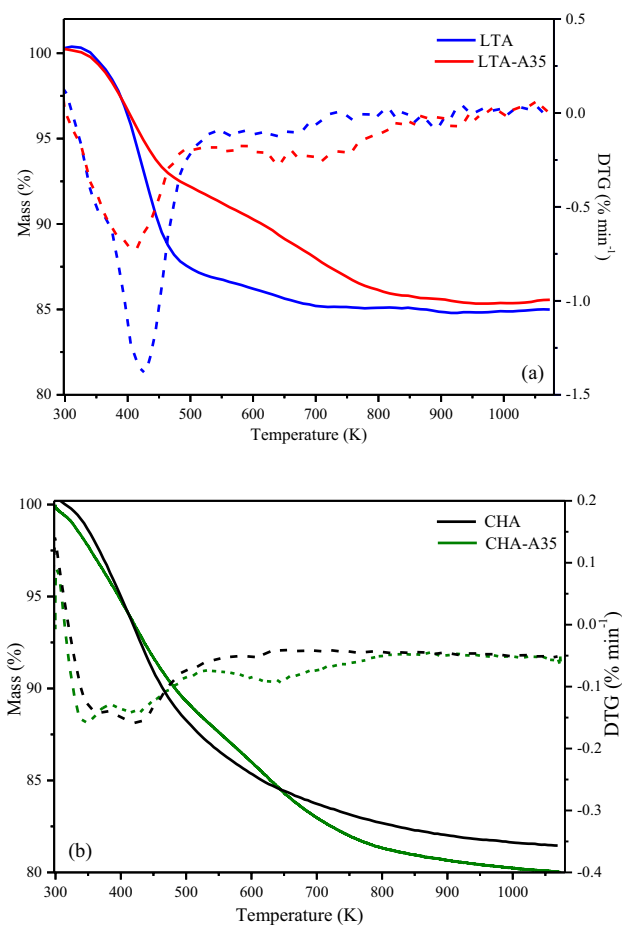
3.7 Water vapor adsorption isotherm at 303 K

The hydrophilicity of any sorbent can be qualitatively judged based on the shape of the water sorption isotherms [33]. Figure 8 presents the water isotherms at 303 K for LTA and CHA fresh and aged samples. All of the samples show quite rectangular isotherms, which is characteristic of hydrophilic materials that reach high water uptake at low to moderate P/P_0. None of the isotherms reaches a constant plateau as pressure increases, but rather shows a slight and steady rise in the moderate pressure range, escalating significantly close to the saturation pressure. This is indicative of multilayer adsorption within macropores close to the saturation pressure values [16, 33]. These are in agreement with the adsorbent pellet composition, which comprises zeolite crystals and a shaping binder. The water adsorption capacity is generally affected by physical parameters (such
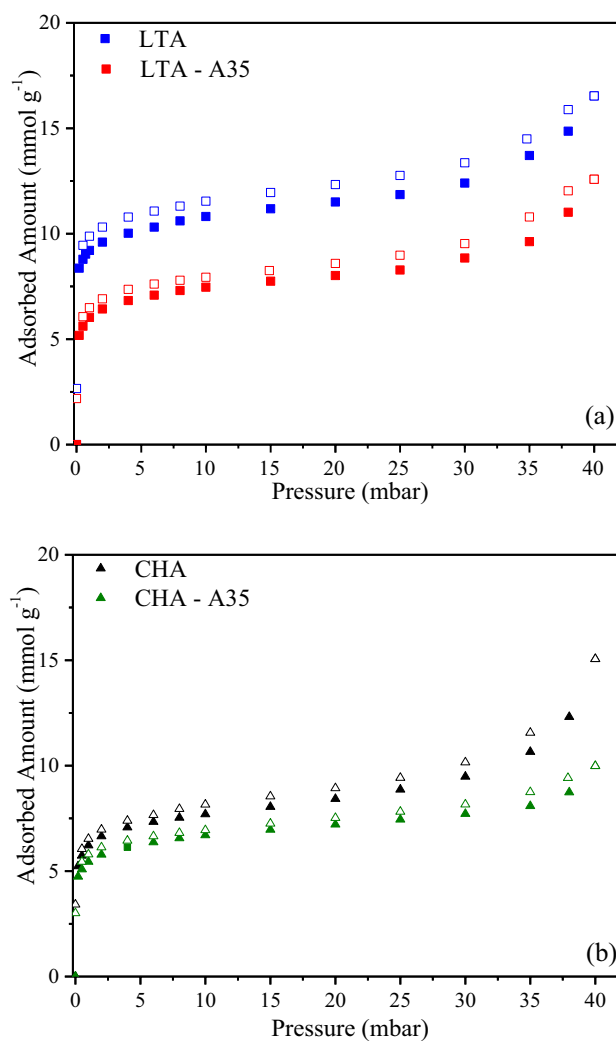

Fig. 7 TGA (Continuous lines) and DTG (dotted lines) of LTA (**a**) and CHA (**b**)

Fig. 8 Vapor water adsorption isotherms at 303 K to the fresh and aged after 35 cycles to LTA samples (**a**) and CHA samples (**b**)

as the specific surface area, micropore volume, pore size) and chemical parameters (Si/Al ratio, compensating cations and substitution of silicon atoms by other elements) [34]. The water uptake of LTA fresh zeolite is 23.6% higher than that of chabazite at 30 mbar (close to $P/P_0 = 0.7$). These results could be associated with the higher cage volume and lower Si/Al ratio of LTA samples in comparison to the CHA samples, taking into account that the binder behaves as an inert filler with negligible water capacity [35]. In fact, it has already been reported that the amount of adsorbed water increases with lower Si/Al ratio [36]. XRF results on Table 2 show that the Si/Al ratio of CHA is twice as much as that of LTA. The adsorption sites for water molecules are the accessible spaces in the vicinity of the exchanged cations and the Si/Al ratio of a zeolite controls the amount of cations and their position in the crystal lattice.

Furthermore, the water heat of adsorption on LTA samples also correlates with the higher affinity of water vapor for LTA as compared to CHA. Close to zero coverage, water heats of adsorption of 90 kJ/mol have been reported for LTA [35] in contrast with 73.6 kJ/mol for CHA [37]. Note that both samples showed a discrete hysteresis loop. The hysteresis loop is probably due to strongly bound water adsorbed by small-pore hydrophilic zeolites, such as LTA and CHA, which ordinarily require temperatures higher than 473 K to be desorbed. At 313 K, the same initial sample mass is not restored even at pressures as low as 5×10^{-4} bar.

The aged sample LTA-A35 suffers almost 30% reduction in water uptake at 30 mbar (P/P_0 around 0.7), as shown on the Fig. 8a. This result could be associated to coke deposition suggested in FTIR and CHN analysis, which induced the micropore volume reduction by cage/pore blocking. This water adsorption reduction is also in agreement with the TGA/DTG curves for this zeolite, as shown in Fig. 7a. For CHA samples, the aging protocol led to a less severe reduction in water adsorption capacity, about 18% at 30 mbar, although it reaches 33% at 40 mbar (close to the saturation pressure at 303 K). By visual inspection of Fig. 8, LTA looks more susceptible to hydrothermal aging as compared to CHA; nonetheless, the two samples aged under the same conditions reached similar water adsorption capacity up to 10 mbar.

Hydrothermal resistance of zeolites might be associated with the adsorbent structure. Fals et al. [38] have studied coke formation in two FAU zeolites with different levels of intracrystalline mesoporosity. The material with the largest mesopore volume showed higher coke content, which was attributed to more available pore volume to host coke precursors within the zeolite [38]. Likewise, the large alpha cages of LTA provide adequate environment for the formation of alkyl-aromatics and PAHs. CHA cages have a smaller volume and tend to allow the formation of smaller molecules [29]. Another key factor is the diffusion of adsorbate species

and/or reaction products in/out of the zeolite cages, which is restricted by the pore opening that leads to the cages. Therefore, zeolites with a hierarchical structure are likely to show higher hydrothermal resistance because they allow for the diffusion of coke out of the structure, which prevents the accumulation of carbonaceous compounds blocking the adsorption sites [29, 38].

3.8 Water adsorption kinetics

The water adsorption uptake in response to a pressure step to 0.25 mbar is shown in Fig. 9 for the fresh and aged LTA samples. The lines represent the solution of the mathematical model taking the diffusion coefficient as the target parameter to fit experimental data. The shape of the curves shows a fast mass increase in the first 5000 s, followed by a slow approach to equilibrium. This behavior is characteristic of systems controlled by energy transfer [39]. The aging test influenced not only water adsorption capacity (equilibrium uptake), but also the transient response (mass transfer kinetics). These are shaped pellets and different mass transfer resistances (micropore and macropore) are lumped in a single parameter D (effective diffusivity), so we chose to report an effective diffusion time constant D/R^2. R is a characteristic diffusion length that is not precisely defined because a global mass transfer parameter is being measured. The values obtained from the model solution curves for the effective diffusion time constant are 6.00×10^{-6} s^{-1} for fresh LTA and 4.21×10^{-6} s^{-1} for the aged sample. These values fall within the same order of magnitude as those found in the literature for this molecular sieve [36]. As expected, the lower water diffusivity of the aged sample is attributed to the pore blocking effect due to the coke accumulation on the zeolite cages.
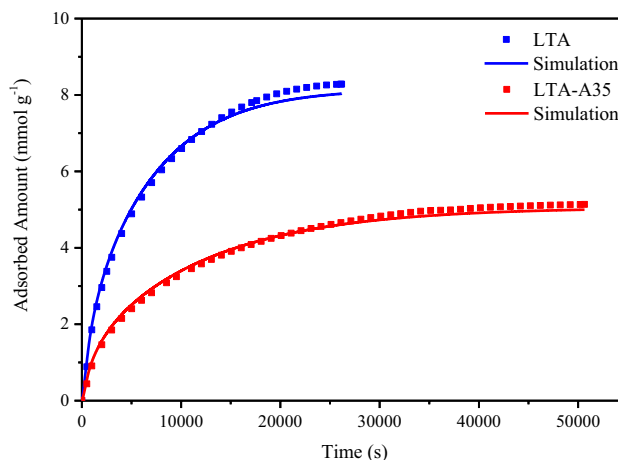

Fig. 9 Vapor water adsorption uptake on LTA samples simulation (line) and experimental data (squares) for the pressure point of 0.25 mbar
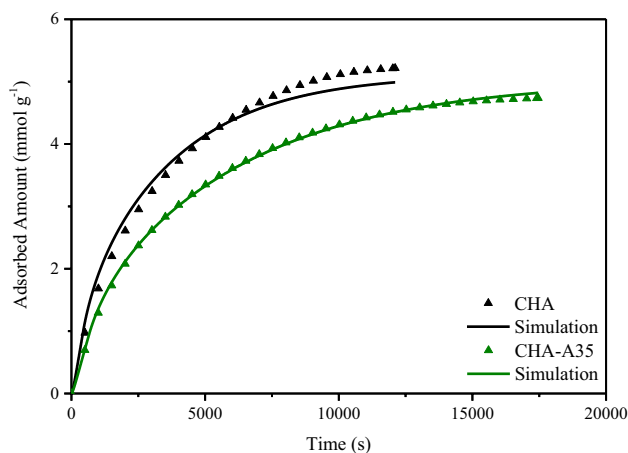
Fig. 10 Vapor water adsorption uptake on CHA samples simulation (line) and experimental data (squares) for the pressure point of 0.25 mbar

Table 5 Effective diffusion time constants of water in LTA and CHA, as estimated from uptake rate curves in response to a pressure step of 0.25 mbar at 303 K

Sample	Effective diffusion time constant $(s^{-1}) \times 10^6$
LTA	6.00
LTA-A35	4.28
CHA	17.5
CHA-A35	7.28

In the case of CHA subject to the same pressure step (Fig. 10), the fresh sample achieves adsorption equilibrium faster than the LTA zeolite, which confirms easier diffusive transport in the zeolite structure. Because both LTA and CHA have similar micropore volumes (CO_2) and pore openings [14], this lower water mobility in LTA seems to be connected to the different Si/Al ratios, which render LTA a higher sorbate/sorbent affinity. The aged CHA sample shows a discreet reduction in water equilibrium uptake and a slower approach to equilibrium, as compared to the fresh sample. The effective diffusion time constant values found were 1.75×10^{-5} and 7.28×10^{-6} s^{-1} for the fresh and aged samples, respectively. All effective diffusion time constants are summarized in Table 5. Although the time constant was reduced more than twofold in the case of CHA, water uptake is still faster in aged CHA than in fresh LTA, which translates into less disperse water concentration fronts in the TSA columns, an important design issue.

4 Conclusions

In this work, two molecular sieves commonly used in natural gas drying (LTA and CHA) were investigated with respect to their hydrothermal resistance by undergoing a laboratory aging protocol that emulates TSA conditions. Both sieves have similar textural characteristics (using CO_2 at 273 K as probe molecule) but different crystal unit cells and Si/Al ratios. FTIR, CHN and TGA analysis indicate the deposition of (alkyl) aromatic compounds in aged LTA and aliphatic compounds in aged CHA, although carbon content in both samples is similar. The fresh LTA zeolite showed a water adsorption capacity 23.6% higher than that of CHA, probably due to a lower Si/Al ratio. On the other hand, LTA zeolite showed to be much more prone to thermal deactivation than CHA, with 28.6% reduction in water uptake in contrast to 18.4% in the CHA sample at 30 mbar. The diffusion of water at low loadings was much faster for fresh CHA than fresh LTA, although the aged samples showed comparable values of effective diffusivity. The lower Si/Al ratio (implying higher surface acidity) and the presence of comparatively larger cages seem to be key factors that render LTA a higher susceptibility to hydrothermal deactivation and lower mobility of water molecules.

References

1. Mokhatab, S., Poe, W.A., Mak, J.Y.: Natural gas dehydration and mercaptans removal. In: Mokhatab, S., Poe, W.A., Mak, J.Y. (eds.) Handbook of Natural Gas Transmission and Processing: Principles and Practices, pp. 307–348. Gulf Professional Publishing, Cambridge (2019)
2. Nastaj, J., Ambrozek, B.: Analysis of gas dehydration in TSA system with multi-layered bed of solid adsorbents. Chem. Eng. Process. **96**, 44–53 (2015)
3. Haque, M.E., Xu, Q., Palanki, S.: Glycol loss minimization for a natural gas dehydration plant under upset conditions. Ind. Eng. Chem. Res. **58**, 1994–2008 (2019)
4. Rouquerol, F., Rouquerol, J., Sing, K.S.W., Llewellyn, P.L., Maurin, G.: Adsorption by Powders and Porous Solids: Principles, Methodology and Applications, 2nd edn. Elsevier/Academic Press, Amsterdam (2014)
5. Berg, F., Pasel, F., Eckardt, T., Bathen, D.: Temperature swing adsorption in natural gas processing: a concise overview. Chem. Biol. Eng. Rev. **3**, 59–71 (2019)

6. Pham, T.D., Liu, Q., Lobo, R.F.: Carbon dioxide and nitrogen adsorption on cation-exchanged SSZ-13 zeolites. Langmuir **29**, 832–839 (2013)

7. Ruthven, D.M.: Principles of Adsorption and Adsorption Processes. Wiley, New York (1984)

8. Thomas, W.J., Crittenden, B.: Adsorption Technology & Design. Butterworth Heinemann, Lymington (1998)

9. Santiago, R.G., Santos, B.F., Lima, I.G., Moura, K.O., Melo, D.C., Grava, W.M., Bastos-Neto, M., de Lucena, S.M.P., de Azevedo, D.C.S.: Investigation of premature aging of zeolites used in the drying of gas streams. Chem. Eng. Commun. **206**, 1378–1385 (2019)

10. Do, D.D.: Adsorption Analysis: Equilibria and Kinetics. Imperial College Press, London (1998)

11. Siqueira, R.M., Vilarrasa-García, E., Torres, A.E.B., de Azevedo, D.C.S., Bastos-Neto, M.: Simple procedure to estimate mass transfer coefficients from uptake curves on activated carbons. Chem. Eng. Technol. **41**, 1622–1630 (2018)

12. Kärger, J., Ruthven, D.M.: Diffusion in nanoporous materials: Fundamental principles, insights and challenges. New. J. Chem. **40**, 4027–4048 (2016)

13. Wang, J.-Y., Mangano, E., Brandani, S., Ruthven, D.M.: A review of common practices in gravimetric and volumetric adsorption kinetic experiments. Adsorption **27**, 295–318 (2021)

14. Database of zeolite structure. Structure Commission of the International Zeolite Association (IZA-SC). http://www.iza-structure.org/databases/ (2017). Accessed 30 March 2021

15. Zamechek, W.: Determination of the Elemental Compositor of Zeolitic Materials: Verified Syntheses of Zeolitic Materials, pp. 51–53. Elsevier, Amsterdam (2001)

16. Thommes, M., Kaneko, K., Neimark, A.V., Olivier, J.P., Rodriguez-Reinoso, F., Rouquerol, J., Sing, K.S.W.: Physisorption of gases, with special reference to the evaluation of surface area and pore size distribution (IUPAC Technical Report). Pure Appl. Chem. **87**, 1051–1069 (2015)

17. Jensen, N.K., Rufford, T.E., Watson, G., Zhang, D.K., Chan, K.I., May, E.F.: Screening zeolites for gas separation applications involving methane, nitrogen, and carbon dioxide. J. Chem. Eng. Data **57**, 106–113 (2012)

18. Seabra, R., Ribeiro, A.M., Gleichmann, K., Ferreira, A.F.P., Rodrigues, A.E.: Adsorption equilibrium and kinetics of carbon dioxide, methane and nitrogen on binderless zeolite 4A adsorbents. Microporous Mesoporous Mater. **277**, 105–114 (2019)

19. Tounsi, H., Mseddi, S., Djemel, S.: Preparation and characterization of Na-LTA zeolite from Tunisian sand and aluminum scrap. Phys. Procedia **2**, 1065–1074 (2009)

20. Valiullin, R., Kärger, J., Cho, K., Choi, M., Ryoo, R., et al.: Dynamics of water diffusion in mesoporous zeolites. Microporous Mesoporous Mater. **142**, 236–244 (2011)

21. Zavareh, S., Farrokhzad, Z., Darvishi, F.: Modification of zeolite 4A for use as an adsorbent for glyphosate and as an antibacterial agent for water. Ecotoxicol. Environ. Saf. **155**, 1–8 (2018)

22. Moreira, J.C., Santa, R.A.A.B., Miraglia, G.L., Soares, C., Riella, H.G.: Evaluation of different reaction systems to obtain zeolite 4A via reverse microemulsion. Microporous Mesoporous Mater. **279**, 262–270 (2019)

23. Kim, W., Choi, D., Kim, S.: Sonochemical synthesis of zeolite A from metakaolinite in NaOH solution. Mater. Trans. **51**(9), 1694–1698 (2010)

24. Markovic, S., Dondur, V., Dimitrijevic, R.: FTIR spectroscopy of framework aluminosilicate structures: carnegieite and pure sodium nepheline. J. Mol. Struct. **654**(1–3), 223–234 (2003)

25. Aysan, H., Edebali, S., Ozdemir, C., Karakaya, M.C., Karakaya, N.: Use of chabazite, a naturally abundant zeolite, for the investigation of the adsorption kinetics and mechanism of methylene blue dye. Microporous Mesoporous Mater. **235**, 78–86 (2016)

26. Geng, H., Li, G., Liu, D., Liu, C.: Rapid and efficient synthesis of CHA-type zeolite by interzeolite conversion of LTA-type zeolite in the presence of N, N, N-trimethyladamantammonium hydroxide. J. Solid State Chem. **265**, 193–199 (2018)

27. Guisnet, M., Ribeiro, F.R.: Deactivation and Regeneration of Zeolite Catalysts. Imperial College Press, London (2011)

28. Colthup, N.B., Daly, L.H., Wiberley, S.E.: Introduction to Infrared and Raman Spectroscopy, 3rd edn. Academic Press, San Diego (1990)

29. Park, J.W., Seo, G.: IR study on methanol-to-olefin reaction over zeolites with different pore structures and acidities. Appl. Catal. A **356**, 180–188 (2009)

30. Montanari, T., Busca, G.: On the mechanism of adsorption and separation of CO_2 on LTA zeolites: an IR investigation. Vib. Spectrosc. **46**, 45–51 (2008)

31. Xiong, Z., Syed-Hassan, S.S.A., Xu, J., Wang, Y., Hu, S., Su, S., Zhang, S., Xiang, J.: Evolution of coke structures during the pyrolysis of bio-oil at various temperatures and heating rates. J. Anal. Appl. Pyrolysis **134**, 336–342 (2018)

32. Iqbal, A., Sattar, H., Haider, R., Munir, S.: Synthesis and characterization of pure phase zeolite 4A from coal fly ash. J. Clean. Prod **219**, 258–267 (2019)

33. Ng, E.-P., Mintova, S.: Nanoporous materials with enhanced hydrophilicity and high water sorption capacity. Microporous Mesoporous Mater. **114**, 1–26 (2008)

34. Tatlier, M., Munz, G., Henninger, S.K.: Relation of water adsorption capacities of zeolites with their structural properties. Microporous Mesoporous Mater. **264**, 70–75 (2018)

35. Wang, Y.: Measurements and modeling of water adsorption isotherms of zeolite linde-type A crystals. Ind. Eng. Chem. Res. **59**, 8304–8314 (2020)

36. Yamamoto, T., Kim, Y.H., Kim, B.C., Endo, A., Thongprachan, N., Ohmori, T.: Adsorption characteristics of zeolites for dehydration of ethanol: evaluation of diffusivity of water in porous structure. Chem. Eng. J. **181–182**, 443–448 (2012)

37. Jänchen, J., Bish, D.L., Möhlman, D.T.F., Stach, H.: Investigation of the water sorption properties of Mars-relevant micro- and mesoporous minerals. Icarus **180**, 353–358 (2006)

38. Fals, J., García, J.R., Falco, M., Sedran, U.: Coke from SARA fractions in VGO. Impact on Y zeolite acidity and physical properties. Fuel **225**, 26–34 (2018)

39. Ruthven, D.M.: Diffusion in type A zeolites: New insights from old data. Microporous Mesoporous Mater. **162**, 69–79 (2012)

40. Dawoud, B., Vedder, U., Amer, E.-H., Dunne, S.: Non-isothermal adsorption kinetics of water vapour into a consolidated zeolite layer. Int. J. Heat Mass Transf. **50**, 2190–2199 (2007)

41. Qiu, L., Murashov, V., White, M.A.: Zeolite 4A: heat capacity and thermodynamic properties. Solid State Sci. **2**, 841–846 (2000)

42. Chipera, S.J., Bish, D.L., Carlos, B.A.: Equilibrium modeling of the formation of zeolites in fractures at Yucca Mountain, Nevada. Natural Zeolites '93: Occurrence, Properties, Use, pp. 565–577 (1995)

43. Jänchen, J., Stach, H., Hellwig, U.: Water sorption in faujasite- and chabazite type zeolites of varying lattice composition for heat storage applications. Stud. Surf. Sci. Catal. **174**, 599–602 (2008)

44. Barrer, R.M., Fender, B.E.F.: The diffusion and sorption of water in zeolites-II. Intrinsic and self-diffusion. J. Phys. Chem. Solids **21**, 12–24 (1961)

Publisher's Note Springer Nature remains neutral with regard to jurisdictional claims in published maps and institutional affiliations.